RSC Advances

PAPER

View Article Online
View Journal | View Issue

Cite this: *RSC Adv.*, 2015, **5**, 88209

Fabrication and photoelectrochemical properties of silicon/nickel oxide core/shell nanowire arrays†

Fu-Qiang Zhang,[a] Ya Hu,[a] Xiang-Min Meng[b] and Kui-Qing Peng*[a]

Received 3rd August 2015
Accepted 9th October 2015

DOI: 10.1039/c5ra13857d

www.rsc.org/advances

A photoelectrochemical (PEC) cell made of a silicon nanowire array coated with a thin nickel oxide (NiO_x) shell layer for solar water oxidation is presented. The silicon/NiO_x core/shell nanowire photoanodes are fabricated by a simple and scalable one-step galvanic displacement reaction and thermal annealing. The conformal NiO_x shell layer functions as an oxygen evolution catalyst to reduce the onset potential as well as a protection layer against corrosion. It was found that about 30 nanometer thick NiO_x film coated p-type silicon nanowire arrays exhibited efficient water oxidation activity with stability for more than 48 h in aqueous Na_2SO_4 solution (pH ~ 7). The scalability of this approach is promising for the fabrication of Si-based photoelectrodes.

1. Introduction

In recent decades, solar water splitting into hydrogen and oxygen has attracted considerable attention because of the global energy crisis and for environmental sustainability.[1–3] As one of the half reactions of water splitting, the oxygen evolution reaction (OER) is a complex proton-coupled electron transfer (PCET) process. However, the complex PCET process is sluggish and typically requires additional overpotential for solar water splitting. The development of economical catalysts with stable, high performance in solution remains a challenge. High light absorption, fast electron–hole separation and well matched interfacial redox reactions are essential for efficient photoelectrochemical (PEC) water oxidation.[4–10] A variety of photocatalysts including Cu_2O, α-Fe_2O_3 (hematite), WO_3 and TiO_2 [11–26] have been investigated for efficient PEC solar water oxidation.

Due to its efficient visible light absorption ability, high carrier mobility and earth abundance, silicon is widely used for photovoltaic applications, but its two distinct disadvantages limit its practical application in solar water splitting. Specifically, silicon easily suffers from photocorrosion in aqueous electrolytes[27] and its relatively high valence band edge position makes it not suitable for water oxidation. Many efforts have been made to overcome these problems, such as passivating the silicon surface with metal/metal oxide,[28,29] organic polymer[30–32] and wide band gap semiconductors.[33–38] Sun *et al.* showed silicon functionalized with nickel oxide for efficient water oxidation with good stability.[39] Reece *et al.* showed an efficiencies of 2.5% for wireless water splitting device with 10 hours stability.[23] Liu *et al.* showed a fully integrated nanosystem which achieves 0.12% solar-to-fuel conversion efficiency.[40] Due to its earth abundance and compatible with the industry, nickel oxide is considered to be one of the best OER catalysts.[41] Sol–gel method has been widely used to synthesize the NiO_x film.[42,43] But the sol–gel method is not suitable to prepare conformal silicon/NiO_x core/shell nanowire arrays due to the narrow space among silicon nanowires.[44,45]

In this work, we demonstrate a simple and cheap method to fabricate three-dimensional (3D) conformal silicon/NiO_x core–shell nanowire arrays for solar water splitting. The method is based on the Ni–Si displacement reaction in aqueous solution.[46,47] The higher work function of NiO_x made it more suitable for water oxidation than Ni. Silicon nanowire core layer plays the role of efficient light absorption, provides fast charge transfer and large area chemical reaction centre while the shell layer NiO_x film serves as OER catalyst and protective layer. The PEC properties of the Si/NiO_x core/shell nanowire photoanodes are systematically investigated.

2. Experimental section

2.1. Fabrication of silicon nanowire arrays

The fabrication of silicon/NiO_x core/shell nanowire arrays is schematically illustrated in Fig. S1.† Aligned single-crystalline silicon nanowire (SiNW) arrays are prepared on Si wafers by means of electroless etching of silicon in aqueous HF–$AgNO_3$ solution.[44] First, 2 × 2 cm^2 *p*-Si(100) (B doped, 1–10 Ω cm) pieces are ultrasonically degreased in acetone and ethanol for 10 minutes, respectively. Second, the silicon wafer was immersed in a boiling solution of H_2SO_4/H_2O_2 for 30 minutes. After

[a]*Department of Physics and Beijing Key Laboratory of Energy Conversion and Storage Materials, Beijing Normal University, Beijing, 100875, China. E-mail: kq_peng@bnu.edu.cn*

[b]*Technical Institute of Physics and Chemistry and Key Laboratory of Photochemical Conversion and Optoelectronic Materials, Chinese Academy of Sciences, Beijing, 100190, China*

† Electronic supplementary information (ESI) available. See DOI: 10.1039/c5ra13857d

cooling in the atmosphere, the wafers were taken out and thoroughly rinsed with DI water. Third, the clean silicon pieces were immersed in aqueous HF/$AgNO_3$ solution (0.25 M $AgNO_3$, 40%HF solution) for etching about 30 minutes. Then, the produced SiNW array samples were immersed in concentrated nitric acid (65%) for 30 min to remove residual Ag. After removing the oxide layer with diluted HF solution (1.0%) and rinsed with DI water, the samples were dried in the air at room temperature.

2.2. Fabrication of silicon/nickel oxide core/shell nanowire photoanodes

First, $NiSO_4 \cdot 6H_2O$ (14.74 g), NH_4F (5.18 g), $(NH_4)_2SO_4$ (3.70 g) and 0.01 g sodium dodecyl sulfate were mixed in 50 mL of DI water at 60 °C. After stirring for 10 min, NH_4OH was added to adjust the pH value to 7.5. Second, the as prepared SiNWs samples were immersed in the mixture solution for 5 minutes. The galvanic displacement reaction between nickel ions and silicon atoms immediately occurs. Nickel ions were reduced and deposited as metallic Ni on silicon nanowire surface, as shown in Fig. S1b.† Then the samples were immersed in acetone for 24 h to remove the residue resistant plastic layer and rinsed with DI water. Third, the silicon/nickel core/shell nanowire samples were annealed in a horizontal tube furnace at450 °C for 40 minutes under atmospheric environment and *in situ* formed nickel oxide film was uniformly coated on the SiNWs surface as shown in Fig. S1c.†

2.3. Characterization

The samples were characterized by scanning electron microscopy (SEM, HITACHI S4800), transmission electron microscopy (TEM, JEOL JEM2100), UV-visible spectrometry (Carry5000, Agilent), X-ray diffraction (XRD) using Cu Kα radiation (Rigiku, Japan) and X-ray photoelectron spectroscopy (ESCSLAB 250Xi, ThermoFisher). The photoelectrochemical measurements were performed in a custom-made electrochemical cell with a 1.0 cm^2 quartz window using a Zennium electrochemical workstation (IM6, Zahner) with platinum wire coil as counter electrode. A 500 W Xe lamp was used to provide 1 sun (100 mW cm^{-2}) illumination to the sample. The electrolyte is 0.5 M Na_2SO_4 aqueous solution (pH ~ 7). The incident photo to current efficiency (IPCE) was measured using Newport's IQE 200 system. The evolved gas was characterized using a Gas Chromatography (GC 7890B Agilent) with H_2 as the carried gas.

3. Results and discussion

Fig. 1a and b respectively show the top-view and cross-section SEM images of as-prepared Si/NiO_x core/shell nanowire arrays (all the composite photoanodes reported herein are prepared by 5 min displacement reaction, unless otherwise noted). The nanowires have lengths of about 3 μm and diameters varied from 20–300 nm. The SEM images show no obvious agglomeration of the nanowires after displacement reaction and thermal annealing. The SiNWs are conformal coated with uniform NiO_x film from top to bottom. The particles observed in the

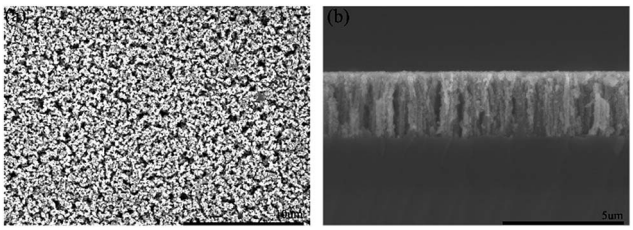

Fig. 1 (a) Top view and (b) cross section scanning electron micrograph images of silicon/NiO_x core/shell nanowire arrays.

surface of the nanowires are nickel oxide, which is in agreement with previous report.[46,47] It should be noted that the planar silicon is hard to react with nickel ion by this displacement reaction because of its inactive surface. Planar silicon had to be textured to enhance the surface. The thin nanostructure layer on the planar silicon is prepared by the Ag-catalysed electroless etching method, but the etching time is decreased to 2 min. The thickness of the textured layer on planar silicon is about 400 nm.

Fig. 2a shows the XRD pattern of the as-prepared silicon/NiO_x core/shell nanowire arrays. The peak at the angle of 33° is the second diffraction peak of Si (400). The XRD data implies the presence of (111), (200) and (220) NiO diffraction peaks, (202) and (004) Ni_2O_3 diffraction peaks, indicating most of the peaks correspond to NiO_x and silicon substrate. Fig. 2b shows the UV-vis absorption spectra of silicon/NiO_x core/shell nanowire arrays prepared by different displacement reaction time. The as-prepared silicon/NiO_x core/shell nanowire arrays show excellent broadband light absorption from 300 nm to 1100 nm. The light absorption ability gradually decreases with the increase of displacement reaction time. This can be understood that nickel oxide has a wide band gap of 3.6–4.0 eV which limit its efficient light absorption.[48] The volume and mass percentage of nickel oxide increase with the reaction time, the thick nickel oxide shell layer leads to the overall decrease of light absorption.

The microstructures of as-prepared silicon/NiO_x core/shell nanowires were characterized by transmission electron microscope (TEM). Fig. S2† shows the TEM images of the silicon nanowire after 2 min displacement reaction. It can be seen that the thickness of nickel oxide shell layer is not uniform and even some areas of nanowire surface are nude due to short displacement reaction. This can be further confirmed by the

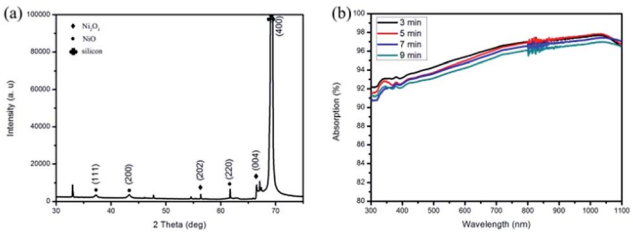

Fig. 2 (a) XRD pattern of silicon/NiO_x core/shell nanowire arrays. (b) UV-vis absorption spectra of silicon/NiO_x core/shell nanowire arrays prepared by different displacement reaction time.

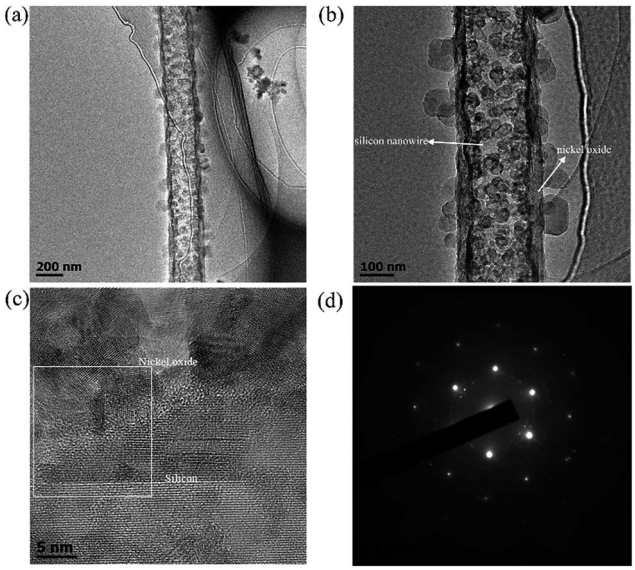

Fig. 3 (a) and (b) TEM images of silicon/NiO_x core/shell nanowire arrays. (c) High Resolution Transmission Electron Microscopy (HRTEM) image of nickel oxide/silicon core/shell layer. (d) Selected area electron diffraction (SAED) of the nanowire.

photograph as shown in Fig. S3.† There are some black areas on the surface of the sample, which represents the unreacted silicon nanowires. In contrast, the right photograph of sample prepared by 5 min displacement reaction shows the sample is coated by uniform nickel oxide film. Fig. 3a and b show the TEM images of the silicon nanowire after 5 min displacement reaction. It can be clearly observed that the SiNW is conformal coated by nickel oxide film with the thickness of about 30 nm. Fig. 3c shows the high resolution transmission electron microscopy (HRTEM) image of the silicon/NiO_x core/shell layer, the crystalline faceting of nickel oxide and silicon is clearly shown. Fig. 3d shows the selected area electron diffraction (SAED) of the nanowire, which further confirms the nickel oxide and silicon layer. The SAED image of the particles on the nanowire is shown in Fig. S4,† the polycrystalline electron diffraction confirms the particles are nickel oxide.

X-ray photoelectron spectroscopy (XPS) was used to analyse the surface chemistry of the annealed samples. Fig. 4a and b show the XPS spectra of O 1s and Ni 2p peaks in the annealed samples, respectively. The O 1s XPS spectrum can be deconvoluted into three peaks with the binding energies of 529.28 eV, 530.97 eV, 532.33 eV, corresponding to the lattice oxygen, the hydroxyl, and surface absorbed water, respectively. The interpretation of Ni 2p spectra is relatively difficult because of complex shakeup and splitting.[49] Here, we used the Gaussian fitting method on the Ni 2p spectrum. The spectrum is fitted with two spin–orbit doublets, characteristics of Ni^{2+} and Ni^{3+}, and two shakeup satellites. The results demonstrate that the composite sample contains Ni^{2+} and Ni^{3+}. The fitting result is consistent with previous reports.[50–52]

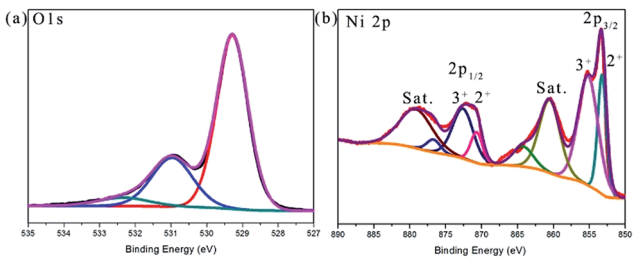

Fig. 4 XPS spectra of silicon/NiO_x core/shell nanowire arrays: (a) O 1s and (b) Ni 2p.

The photoelectrochemical properties of the silicon/NiO_x core/shell nanowire arrays photoanode were investigated in 0.5 M Na_2SO_4 aqueous electrolyte using a custom-made photoelectrochemical cell with Pt wire coil as the counter electrode. The electrodes were immersed in a Teflon cell with a 1.0 cm^2 quartz window for light illumination. The photoelectrochemical properties of silicon/nickel core/shell nanowire electrode were also studied for comparison. No evident difference between dark current and photocurrent in silicon/nickel core/shell nanowire photoanode was observed as shown in Fig. 5a, indicating no photocatalytic activity of the sample. It can be understood that the photoexcited electron–hole pairs recombined immediately before into the circuit. Fig. 5b shows the consecutive multiple linear scan curve of silicon/NiO_x core/shell nanowire photoanode in a two-electrode electrochemical system. The difference between dark current and photocurrent shows the photocatalytic activity of water oxidation and the little difference between the photocurrent curves during the consecutive multiple linear scan indicates the silicon/NiO_x core/shell nanowire photoanode is stable. The relatively high dark current in the photoanode may be due to Seebeck effect, as the temperature difference between the core layer and shell layer. The SiNWs/NiO_x composite photoanode shows 0.036 mA cm^{-2} photocurrent density at 0 V and oxygen bubbles can be observed during the test (Fig. S5†). For comparison, a three-electrode

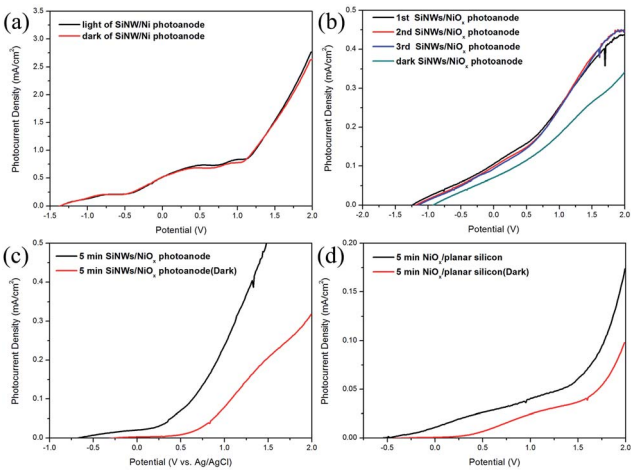

Fig. 5 (a) *J*–*E* curves of silicon/nickel core/shell nanowire arrays. (b) *J*–*E* curves of silicon/NiO_x core/shell nanowire photoanode after three consecutive line sweep scans in two-electrode electrochemical system. (c) *J*–*E* curves silicon/NiO_x core/shell nanowire photoanode in three-electrode electrochemical system with Ag/AgCl as reference electrode. (d) *J*–*E* curves of NiO_x/planar silicon photoanode for comparison.

electrochemical system was adopted to investigate the photoelectrochemical performance of the photoanode (Fig. 5c). The sample served as the working electrode, Pt wire coil served as the counter electrode and the Ag/AgCl with 3 M KCl solution served as the reference electrode. The relative high dark current in two-electrode electrochemical system decreased obviously in three-electrode electrochemical system. Moreover, the onset potential of the photoanode is about −0.7 V *vs.* Ag/AgCl and far more below the thermodynamic oxidation level of water, indicating efficient water oxidation performance of the photoanode. The surface modification and the core/shell nanostructure may be responsible for the low onset potential. The photoexcited electrons in the nickel oxide transport to the conduction band of silicon and then to the circuit; while the photoexcited holes in the nickel oxide oxidize water. The Ni^{2+} and Ni^{3+} ions will participate in the photocatalytic reaction as the mechanism described below.[39]

$$Ni(2/3) + H_2O + h^+ \rightarrow Ni(2/3)(OH) + H^+ \quad (1)$$

$$2Ni(2/3)(OH) \rightarrow Ni(2/3)(O) + Ni(2/3) + H_2O \quad (2)$$

$$2Ni(2/3)(O) \rightarrow 2Ni(2/3) + O_2\uparrow \quad (3)$$

where Ni(2/3) represents the Ni^{2+} or Ni^{3+} active site of nickel. Although the photocurrent of the SiNWs/NiO_x core/shell nanowire photoanode is not ideal compared with other photoanode, but the performance of our photoanode still showed significant progress compared with previous reported nickel oxide nanostructure.

The performance of nickel oxide/planar silicon photoanode was also investigated for comparison. Fig. 5d shows the *J–E* curve of the nickel oxide/planar silicon photoanode and the photocurrent density at 0 V is 0.01 mA cm^{-2}.

In order to further evaluate the PEC performance of silicon/NiO_x photoanode, incident photon to current conversion efficiency (IPCE) measurements were conducted at the potential of 0 V in 0.5 M Na_2SO_4 (Fig. 6a). It can be seen the curve of silicon/NiO_x composite photoanode exhibited obvious enhancement at the wavelength from 360 to 700 nm. The maximum IPCE was 0.68% at 360 nm.

The stability of photoanode is essential for practical solar fuel production. Herein, we design a stability test simulating the daily practical use of the silicon/NiO_x core/shell nanowire photoanode. The test is a chronoamperometric (*J–t*) operation under periodicity simulated light and dark. The light intensity is 100 mW cm^{-2} and the test is conducted in 0.5 M Na_2SO_4 solution. The light/dark one cycle (*T*) is consist of 12 h light illumination (*T*/2) and 12 h dark (*T*/2) in the solution. Fig. 6b shows the *J–E* curve of silicon/NiO_x core/shell nanowire photoanode during different test time. It was found that the silicon/NiO_x core/shell nanowire photoanode maintains stable photoactivity for water oxidation at least 48 h in the solution. The stability of the silicon/NiO_x photoanode by 5 min displacement reaction was further confirmed by SEM observation after the 48 h stability test (Fig. S6†). No noticeable changes or damages of the silicon/NiO_x core/shell nanowire structure were observed after 48 h stability test, further showing the long-time stability of the nanostructure.

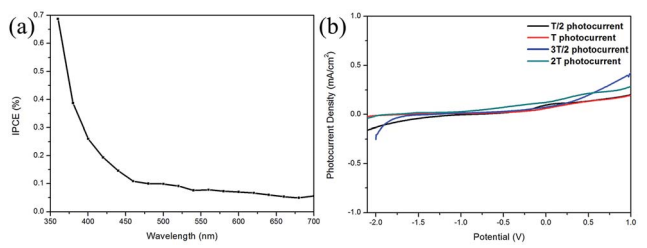

Fig. 6 (a) IPCE curve of silicon/NiO_x core/shell nanowire photoanode. (b) *J–E* curves of silicon/NiO_x core/shell nanowire photoanode during stability test.

4. Conclusion

In conclusion, we have developed a silicon/nickel oxide core/shell nanowires photoanode for efficient solar water oxidation. The NiO_x shell layer functions as oxygen evolution catalyst to reduce onset potential as well as protection layer against corrosion. The photoanode exhibits a low onset potential, relatively high photocurrent density and long-time stability in solution compared with other nickel oxide based structures. More importantly, the photoanode is fabricated by a simple and cost effective method. Considering the abundance of the materials and the scalable production, this approach is promising for the fabrication of Si-based photoelectrodes.

Acknowledgements

We acknowledge financial support from National Basic Research Program of China (2012CB932400), Major Program of NSFC (91333208), NSFC (51072025), Beijing Natural Science Foundation (2112021), Beijing Nova Program (2008B24), and the Fundamental Research Funds of the Central Universities (2012LZD02).

Notes and references

1 N. S. Lewis and D. G. Nocera, *Proc. Natl. Acad. Sci. U. S. A.*, 2006, **103**, 15729–15735.
2 M. Graetzel, *Acc. Chem. Res.*, 1981, **14**, 376–384.
3 H. B. Gray, *Nat. Chem.*, 2009, **1**, 7.
4 Y. J. Hwang, A. Boukai and P. D. Yang, *Nano Lett.*, 2009, **9**, 410–415.
5 B. S. Brunschwig, H. A. Atwater and N. S. Lewis, *J. Am. Chem. Soc.*, 2011, **133**, 1216–1219.
6 J. H. Park, S. Kim and A. J. Bard, *Nano Lett.*, 2006, **6**, 24–28.
7 J. Shi, Y. Hara, C. L. Sun, M. A. Anderson and X. D. Wang, *Nano Lett.*, 2011, **11**, 3413–3419.
8 K. Jun, Y. S. Lee, T. Buonassisi and J. M. Jacobson, *Angew. Chem., Int. Ed.*, 2011, **50**, 423–427.
9 S. D. Tilley, M. Cornuz, K. Sivula and M. Gratzel, *Angew. Chem., Int. Ed.*, 2010, **122**, 6549–6552.
10 S. W. Boettcher, J. M. Spurgeon, M. C. Putnam, E. L. Warren, D. B. Turner-Evans, M. D. Kelzenberg, J. R. Maiolo, H. A. Atwater and N. S. Lewis, *Science.*, 2010, **327**, 185–187.

11 C. Y. Lin, Y. H. Lai, D. Mersch and E. Reisner, *Chem. Sci.*, 2012, **3**, 3482–3487.
12 M. Hara, T. Kondo, M. Komoda, S. Ikeda, K. Shinohara, A. Tanaka, J. N. Kondo and K. Domen, *Chem. Commun.*, 1998, 357–358.
13 P. E. Jongh, D. Vanmaekelbergh and J. J. Kelly, *Chem. Commun.*, 1999, 1069–1070.
14 A. Paracchino, V. Laporte, K. Sivula, M. Gratzel and E. Thimsen, *Nat. Mater.*, 2011, **10**, 456–461.
15 M. T. Mayer, C. Du and D. W. Wang, *J. Am. Chem. Soc.*, 2012, **134**, 12406–12409.
16 Y. J. Lin, Y. Xu, M. T. Mayer, Z. I. Simpason, G. McMahon, S. Zhou and D. W. Wang, *J. Am. Chem. Soc.*, 2012, **134**, 5508–5511.
17 R. H. Coridan, K. A. Arpin, B. S. Brunschwig, P. V. Braun and N. S. Lewis, *Nano Lett.*, 2014, **14**, 2310–2317.
18 S. J. Guo, D. G. Li, H. Y. Zhu, S. Zhang, N. M. Markovic, V. R. Stamenkovic and S. H. Sun, *Angew. Chem., Int. Ed.*, 2013, **52**, 3465–3468.
19 Y. Y. Liang, Y. G. Li, H. L. Wang, J. G. Zhou, J. Wang, T. Regier and H. J. Dai, *Nat. Mater.*, 2010, **10**, 780–786.
20 D. A. Wang, T. Hisatomi, T. Takata, C. S. Pan, M. S. Katayama, J. Kubota and K. Domen, *Angew. Chem., Int. Ed.*, 2013, **52**, 11252–11256.
21 G. M. Wang, Y. C. Ling, D. A. Wheeler, K. N. George, K. Horsley, C. Heske, J. Z. Zhang and Y. Li, *Nano Lett.*, 2011, **11**, 3503–3509.
22 L. Liao, Q. H. Zhang, Z. H. Su, Z. Z. Zhao, Y. N. Wang, Y. Li, X. X. Lu, D. G. Wei, G. Y. Feng, Q. K. Yu, X. J. Cai, J. M. Zhao, Z. F. Ren, H. Fang, F. R. Hernandez, S. Baldelli and J. Bao, *Nat. Nanotechnol.*, 2013, **9**, 69–73.
23 S. Y. Reece, J. A. Hamel, K. Sung, T. D. Jarvi, A. J. Esswein, J. H. Pijpers and D. G. Nocera, *Science.*, 2011, **334**, 645–648.
24 X. Yu, X. Han, Z. H. Zhao, J. Zhang, W. B. Guo, C. F. Pan, A. X. Li, H. Liu and Z. L. Wang, *Nano Energy*, 2015, **11**, 19–27.
25 Y. Yang, H. L. Zhang, Z. H. Lin, Y. Liu, J. Chen, Z. Y. Lin, Y. S. Zhou, C. P. Wong and Z. L. Wang, *Energy Environ. Sci.*, 2013, **6**, 2429–2434.
26 X. P. Qi, G. W. She, M. Wang, L. X. Mu and W. S. Shi, *Chem. Commun.*, 2013, **49**, 5742–5744.
27 H. Gerischer, *Faraday Discuss. Chem. Soc.*, 1980, **70**, 137–151.
28 K. Sun, X. L. Pang, S. H. Shen, X. Q. Qian, J. S. Cheung and D. L. Wang, *Nano Lett.*, 2013, **13**, 2064–2072.
29 B. Mei, B. Seger, T. Pedersen, M. Malizia, O. Hansen, L. Chorkendorff and P. K. Vesborg, *J. Phys. Chem. Lett.*, 2014, **5**, 1948–1952.
30 T. Yang, H. Wang, X. M. Ou, C. S. Lee and X. H. Zhang, *Adv. Mater.*, 2012, **24**, 6199–6203.
31 R. Noufi, A. J. Frank and A. J. Nozik, *J. Am. Chem. Soc.*, 1981, **103**, 1850–1851.
32 M. D. Rosenblum and N. S. Lewis, *J. Phys. Chem.*, 1984, **88**, 3103–3107.
33 X. Wang, K. Q. Peng, Y. Ha, F. Q. Zhang, B. Hu, L. Li, M. Wang, X. M. Ming and S. T. Lee, *Nano Lett.*, 2014, **14**, 18–23.
34 Y. J. Hwang, A. Boukai and P. D. Yang, *Nano Lett.*, 2009, **9**, 410–415.
35 Y. W. Chen, J. D. Prange, S. Duhnen, Y. H. Park, M. Gunji, C. D. Chidsey and P. C. Mclntre, *Nat. Mater.*, 2011, **10**, 539–544.
36 E. R. Young, R. Costi, S. Paydavosi, D. G. Nocera and V. Bulovic, *Energy Environ. Sci.*, 2011, **4**, 2058–2061.
37 J. H. Pijpers, M. T. Winkler, Y. Surenranath, T. Buonassisi and D. G. Nocera, *Proc. Natl. Acad. Sci.*, 2011, **25**, 10056–10061.
38 A. Kargar, K. Sun, Y. Jing, C. M. Choi, H. S. Jeong, Y. C. Zhou, K. Madsen, P. Naughton, S. Jin, G. Y. Jung and D. L. Wang, *Nano Lett.*, 2013, **13**, 3017–3022.
39 K. Sun, N. Park, Z. L. Sun, J. G. Zhou, J. Wang, X. L. Pang, S. H. Shen, S. Y. Noh, Y. Jing, S. Jin, P. L. Yu and D. L. Wang, *Energy Environ. Sci.*, 2012, **5**, 7872–7877.
40 C. Liu, J. Y. Tang, H. M. Chen, B. Liu and P. D. Yang, *Nano Lett.*, 2013, **13**, 2989–2992.
41 R. L. LeBoy, *Int. J. Hydrogen Energy*, 1983, **8**, 401–417.
42 J. L. Garcia-Miquel, Q. Zhang, S. J. Allen, A. Rougier, A. Blyr, H. O. Davies, A. C. Jones, T. J. Leedham, P. A. Williams and S. A. Impey, *Thin Solid Films*, 2003, **424**, 165–170.
43 P. A. Williams, A. C. Jones, J. F. Bickley, A. Steiner, H. O. Davies, T. J. Leedham, S. A. Impey, J. Garcia, S. Allen, A. Rougier and A. Blyr, *J. Mater. Chem.*, 2001, **11**, 2329–2334.
44 K. Q. Peng, Y. J. Yan, S. P. Gao and J. Zhu, *Adv. Mater.*, 2002, **14**, 1164–1167.
45 K. Q. Peng, M. L. Zhang, A. J. Lu, N. B. Wong, R. Q. Zhang and S. T. Lee, *Appl. Phys. Lett.*, 2007, **90**, 163123.
46 X. Zhang, K. N. Tu, Y. H. Xie, C. H. Tung and S. Y. Xu, *Adv. Mater.*, 2006, **18**, 1905–1909.
47 X. Zhang and K. N. Tu, *J. Am. Chem. Soc.*, 2006, **128**, 15036–15037.
48 H. Yang, Q. Tao, X. Zhang, A. Tang and J. Ouyang, *J. Alloys Compd.*, 2008, **459**, 98–102.
49 A. N. Mansour, *Surf. Sci. Spectra*, 1994, **3**, 231–238.
50 R. Ding, L. Qi, M. J. Jia and H. Y. Wang, *Nanoscale*, 2014, **6**, 1369.
51 C. Z. Yuan, J. Y. Li, L. R. Hou, X. G. Zhang, L. F. Shen and X. W. Lou, *Adv. Funct. Mater.*, 2012, **22**, 4592.
52 K. B. Xu, X. J. Huang, Q. Liu, R. J. Zou, W. Y. Li, X. J. Liu, S. J. Li, J. M. Yang and J. Q. Hu, *J. Mater. Chem. A*, 2014, **2**, 16731.